Data-Driven Feedforward Decoupling Filter Design for Parallel Nanopositioning Stages

Zhao Feng, Jie Ling, Min Ming, and Xiaohui Xiao(✉)

School of Power and Mechanical Engineering,
Wuhan University, Wuhan 430072, China
{fengzhaozhao7, jamesling,
mingmin_whu, xhxiao}@whu.edu.cn

Abstract. Cross-coupling effect severely hinder fast and accurate tracking for parallel piezo nanopositioning stages. In this paper, a data-driven feedforward decoupling filter (DDFDF) is proposed to reduce the cross-coupling caused errors. Traditional control methods for coupled system could achieve good performance on the premise that the dynamic model is accurate and no non-minimum phase zeros exist. The proposed method is totally data-driven with the advantage of no need for accurate identified model and model structure by Gauss-Newton gradient-based algorithm. The DDFDF for eliminating cross-coupling errors was verified on a 2-DOF coupled nanopositioning stage through simulations. Results show the effectiveness of the proposed controller by comparing with open-loop simulations and the well-designed feedback controller.

Keywords: Parallel nanopositioning stage · Cross-coupling effect · Data-driven · Gradient-based algorithm

1 Introduction

The rapid development in nanoscience and nanotechnology has increased the urgent demand for high-speed and high-performance nanopositioning systems [1]. The emergence of flexure-guided, piezoelectric stack-actuated, compact and light nanopositioner that provides repeatable, reliable, and smooth motions meets the requirements for these related applications, such as scanning probe microscopy (SPM) [2], atomic force microscope (AFM) [3], micromanipulation system [4] and so on. There are two kinds of configurations of piezo nanopositioning stage: serial and parallel [5]. For serial-kinematic configuration, only one axis can achieve the high mechanical bandwidth [6]. Parallel structures offer higher resonance frequencies and stiffness on all axes. Therefore, parallel nanopositioning stages have been widely used in commercial design [5].

For parallel nanopositioning stages, cross-coupling among axes inevitably appears and becomes one of the main obstacles for achieving excellent servo performance, especially at high scanning speed, which can be observed from the experiment data presented in [7]. Many special mechanical structures have been designed to reduced cross-coupling effect [8, 9], and the interactive effect can be suppressed significantly at

N. Kubota et al. (Eds.): ICIRA 2016, Part I, LNAI 9834, pp. 709–720, 2016.
DOI: 10.1007/978-3-319-43506-0_61

low frequencies. However, during high-speed motion, the cross-coupling effect still cannot be ignored as inertial effects, especially near the first resonant mode.

Various approaches were proposed to handle the problem. Multiple-input multiple-output (MIMO) damping controllers using reference model matching approach [10, 11] and mixed negative-imaginary and small-gain approach [12] have been designed to damp the first resonant mode and minimize cross-coupling effect simultaneously. Yuen Kuan Yong [13] proposed a H_∞ controller design strategy for each axis regarding the interactive effect as deterministic output disturbance based on the accurate system modeling. To reduce dependence on model, some data-driven controllers using errors obtained from measurement data have been implemented. In [14, 15], iterative feedback tuning (IFT) has been proposed for industrial process control and virtual reference feedback tuning (VRFT) [16, 17] has been implemented to MIMO system with the advantage of one-trial convergence. However, we should note that the controllers above are MIMO feedback design. A more natural configuration would utilize feedforward decoupling part and leave the single-input single-output (SISO) controller part intact.

To avoid feedback loop redundancy and simplify the control system, a feedforward decoupling controller has been designed to compensate for vibration due to interaction in hard disk drives at the cost of accurate modeling in [18]. However, if the plant has non-minimum phase zeros, the controller may be unstable. Besides, the frequency-domain characteristics encompass significant variation from machine-to-machine which cannot be properly modelled. Therefore, we introduce the data-driven feedforward decoupling filter with the advantage of no need for accurate modeling and plant knowledge to suppress the cross-coupling effect. In this paper, the Gauss-Newton algorithm [19] is used to obtain the coefficients of the finite impulse response (FIR) filters by utilize the measurement data like IFT and VRFT. The DDFDF can alleviate problems due to non-minimum phase zeros and the selection of model structure [20] with the aim to provide the conditions that validate a SISO control approach in coupled parallel piezo nanopositioning stage.

The rest of the paper is organized as follows. The cross-coupling effect problems and control scheme are formulated in Sect. 2. The controllers design procedure, including feedback controller, DDFDF are presented in Sect. 3. Simulation results and comparison are presented in Sect. 4 and conclusions are given in Sect. 5.

2 Problem Formulation

In the section, we present the description of the cross-effect as well as the control scheme for corresponding issue.

2.1 Dynamics Model

To simplify the presentation of the coupled parallel piezo nanopositioning stage, a 2×2 diagonal domain plant is considered in this paper, and described as

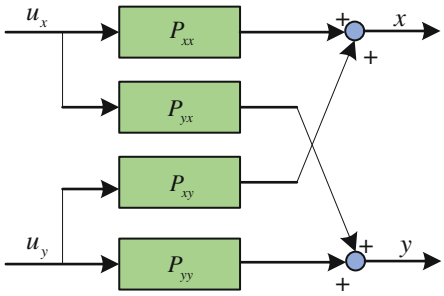

Fig. 1. Dynamics model of a 2 DOFs coupled parallel system

$$P(j\omega) = \begin{bmatrix} P_{xx}(j\omega) & P_{xy}(j\omega) \\ P_{yx}(j\omega) & P_{yy}(j\omega) \end{bmatrix} \tag{1}$$

Figure 1 shows the internal relationship from input to output. Therefore, the coupled parallel dynamics can be modeled as

$$x(\omega) = P_{xx}(j\omega)u_x(\omega) + P_{xy}(j\omega)u_y(\omega) \tag{2}$$

$$y(\omega) = P_{yy}(j\omega)u_y(\omega) + P_{yx}(j\omega)u_x(\omega) \tag{3}$$

Where $x(w)$, $u_x(\omega)$, $y(\omega)$, $u_y(\omega)$ denote the Fourier transforms of $x(t)$, $u_x(t)$, $y(t)$ and $u_y(t)$, respectively. $P_{xx}(j\omega)$ presents the open-loop dynamics of system output x due to the x axis input, and $P_{xy}(j\omega)$ presents the open-loop, cross-coupling effect dynamics under control input $u_y(t)$. Similar definitions are for y axis. To simplify, ω and $|\omega$ are tacitly omitted for conciseness. As we can see from (2) and (3), the output of the individual axis depends on both the diagonal domain dynamics and the cross-coupling dynamic, i.e. non-diagonal domain dynamics, especially at high frequency.

2.2 Control Scheme

For cross-coupling systems, various decoupling feedback methods are proposed to address interactive effect problems [21, 22]. Nevertheless, these existing decoupling feedback control schemes are usually too complex to realize in practical applications, and multi-intersected feedback paths also may render internal uncertainly. Therefore, a common control configuration is a combination SISO feedback control with decoupling feedforward control. The SISO feedback part is to guarantee system robust stability, while the decoupling feedforward part is to attenuate the cross-coupling effect for excellent performance. Figure 2 depicts the configuration of the control system. D_x and D_y are the decoupling feedforward controllers for x axis and y axis. The x axis control input u_x is obtained by subtracting feedback input u_{fbx} from the decoupling feedforward control input u_{dfx} as described in Fig. 2

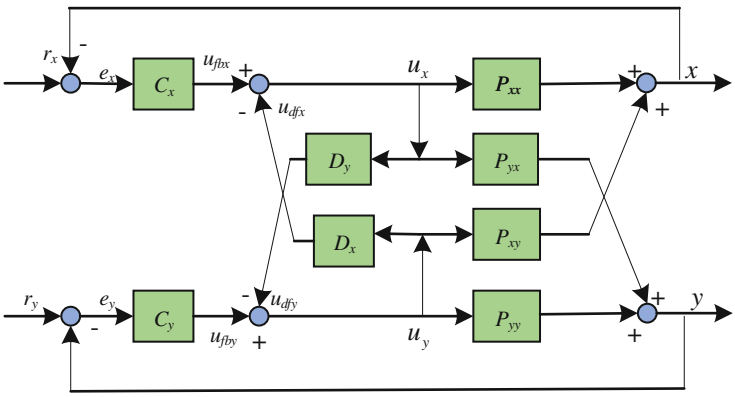

Fig. 2. Configuration of SISO feedback control combined with decoupling feedforward control

$$u_x = u_{fbx} - u_{dfx} \tag{4}$$

The x axis output of the close-loop system can be deduced as

$$x = T_x r_x + S_x P_{xy} u_y - S_x P_{xx} u_{dfx} \tag{5}$$

where T_x, S_x are the complementary sensitivity function and sensitivity function, i.e.

$$T_x = \frac{P_{xx} C_x}{1 + P_{xx} C_x}, \; S_x = \frac{1}{1 + P_{xx} C_x} \tag{6}$$

Therefore, the error of x axis can be described as

$$e_x = S_x r_x - S_x P_{xy} u_y + S_x P_{xx} u_{dfx} \tag{7}$$

Hence, the cross-coupling effect due to u_y can be canceled if

$$-S_x P_{xy} u_y + S_x P_{xx} u_{dfx} = 0 \tag{8}$$

from Eq. (8) the equation can be represented as

$$u_{dfx} = \frac{P_{xy}}{P_{xx}} u_y \tag{9}$$

Therefore, the decoupler of x and y axis is derived as

$$D_x = \frac{P_{xy}}{P_{xx}}, \; D_y = \frac{P_{yx}}{P_{yy}} \tag{10}$$

Through the two decouplers, the parallel system is decoupled into two SISO systems. However, we should note that if P_{xx} or P_{yy} has non-minimum phase zeros,

D_x or D_y is unstable. Therefore, DDFDF is introduced to design the decouplers and a H_∞ controller is implemented to retain robust stability.

3 Controllers Design

In this section, we review the H_∞ controller design briefly. Then a DDFDF is proposed to design the decouplers using the collected data breaking through the limit of accurate modeling and non-minimum phase zeros.

3.1 Feedback Controller

In this paper, the H_∞ controller is designed with the advantage of performance, resolution, and robust to model uncertainty directly considered in the frequency domain via appropriate weighting functions [23]. Now, we consider the H_∞ controller design for x axis. Same is the design for y axis.

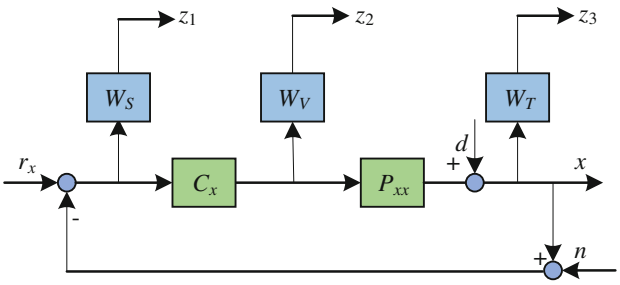

Fig. 3. H_∞ design weighting functions

In H_∞ design the goal is to optimize competing objectives of reference-to-error sensitivity S_x, reference-to-output sensitivity T_x, i.e. complementary sensitivity, and reference-to-control sensitivity C_xS_x simultaneously. The controller C_x is obtained through an iterative design of weighting function to minimize

$$\gamma_{feedback} = \left\| \begin{matrix} W_S S_x \\ W_T T_x \\ W_V C_x S_x \end{matrix} \right\|_\infty \tag{11}$$

where $\|\cdot\|_\infty$ is H_∞ norm. The weighting function W_S, W_T, W_V, which can be seen in Fig. 3, penalize the error, output, and the controller output, respectively; these functions are chosen properly for shaping and obtaining a required close loop transfer function of the controlled system. The details on weighting functions design can be found in [23].

3.2 Data-Driven Feedforward Decoupling Filter Design

In this paper, we chose the FIR filter as the feedforward controllers because of its linear characteristic, which is the essential condition for making the optimal problem convex. The FIR filter structure is defined as

$$D_{ij}(z) = p_0^{ij} + p_1^{ij} z^{-1} + p_2^{ij} z^{-2} + \cdots + p_n^{ij} z^{-n},\ i,j \in \{x,y\} \text{ and } i \neq j \tag{12}$$

With n is the filter order and $p_0^{ij}, p_1^{ij}, p_2^{ij}, \cdots p_n^{ij}$ are its coefficients. Because Eq. (12) represents a numerator polynomial, it has the ability to create zeros inside the unit circle that can approximating the inverse plant dynamics. All the poles located at the origin, which makes the filter stable.

The data-driven feedforward decoupling filter is optimized by a Gauss-Newton gradient-based algorithm. To compensate the cross-coupling errors, the coefficients of FIR filter are obtained by minimizing the objection function. Herein, the objection criterion is chosen as

$$J(k) = e(p^k)^T \lambda e(p^k) \tag{13}$$

where $e(p^k) = \left[e(p^k)_x^T e(p^k)_y^T\right]^T$ donates the cross-coupling errors with respect to the coefficients to be optimized. λ is a diagonal weight matrix. k refers to the iteration number. The algorithm is to obtain the optimal coefficients that satisfies

$$p_n := \arg \min_p J(k) \tag{14}$$

The value of coefficients for each of control directions separately update by a gradient-based algorithm, and the update law can be express as [14]

$$p^{k+1} = p^k - \gamma^k R^{-1} \nabla J|_{p^k} \tag{15}$$

Where R is a certain position definite matrix, i.e. Hessian matrix, and γ donates the step size. The gradient can be derived from object functions as

$$\nabla J|_{p^k} = 2\nabla e(p^k)^T \lambda e(p^k) \tag{16}$$

Herein, we chose the Gauss-Newton method is due to its high convergence rate an accuracy. Therefore, the Hessian matrix can be described as

$$R = \nabla(\nabla J|_{p^k}) \approx 2\nabla e(p^k)^T \lambda \nabla e(p^k) \tag{17}$$

Hence, by substituting (16) and (17), the update law (15) becomes

$$p^{k+1} = p^k - \gamma^k (\nabla e(p^k)^T \lambda \nabla e(p^k))^{-1} \nabla e(p^k)^T \lambda e(p^k) \tag{18}$$

The update law can be seen as strictly data-driven. It requires only the error signal $e(k)$ and the gradient error matrix ∇e which can be obtained from experiment data. Because of the FIR filter coefficients appear affine in the error signals than only one step is need to obtain the optimal set of coefficients from arbitrary initial conditions [24]. To make the optimal method data-driven, the gradient

$$\nabla e(p^k) = [\nabla e(p_0^k) \nabla e(p_1^k) \cdots \nabla e(p_n^k)] \tag{19}$$

is obtained from perturbed-parameter experiment. The first-order Taylor series expansion of the error $e(p^k)$ about the user-defined parameter perturbation difference Δp_i i.e.,

$$e(p^{k+1}) = e(p^k) + \nabla e_i(p^k) \Delta p_i + O(\Delta p_i)^2 \tag{20}$$

Here $e(p^{k+1})$ and $e(p^k)$ are the cross-coupling errors with the perturbation $p_i + \Delta p_i$ and p_i, respectively. Hence, the resulting gradient approximation is given by

$$e_i(p^k) \approx \frac{e(p^{k+1}) - e_i(p^k)}{\Delta p_i} \tag{21}$$

However, the numbers of experiment are large as the coefficient numbers increase because the one experiment is need for each coefficient. To make the optimization technique more suited for practical application, the choice of FIR filter structure is critical. The structure Eq. (12) has a benefit of obtaining the gradient. Once the term $\nabla e_0(p^k)$ is obtained, the whole gradient $\nabla e(p^k)$ can be calculated immediately since the term $\nabla e_n(p^k)$ is equal the term $\nabla e_0(p^k)$ by a delay of i sampling times, i.e.

$$\nabla e_n(p^k) = \nabla e_0(p^k) z^{-i} \tag{22}$$

Hence, only two experiments are made for each direction. This feature simplifies the practical implementation of the algorithm. In summary, the follow procedure is adopted to obtain the FIR filter coefficients.

1. Set the initial FIR filter coefficients p to $p_0^k = 0$.
2. Execute a task and obtain the error signals e_0 from the time-intervals.
3. Perturb the coefficients p^{xy} with Δp_0, excuse the task, and store the signals $e_{xy}(p_0^{k+1})$
4. Use Eq. (21) compute the error gradient $\nabla e_{xy}(p_0^k)$.
5. Apply the time delay Eq. (22) and get $\nabla e_{xy}(p^k)$.
6. Use Eq. (18) obtain the optimal coefficients of D_{xy}.
7. Repeat the $3 \sim 6$ to calculate coefficients of D_{yx}.

4 Evaluation

The following section evaluates the DDFDF through simulation on a 2-DOF parallel piezo nanopositioning stage. The proposed MFDF was verified via the elimination of cross-coupling effect on y axis when triangle signals with difference frequencies were excited to x axis from time domain and frequency domain.

4.1 System Description

A 2-DOF parallel piezo-actuated nanopositioning stage with a stroke of 100 μm × 100 μm was used as the controlled objective. Each of the x and y direction is actuated by a PZT and The displacement of each axis is detected by a capacitive sensor with the close loop resolution of 10 nm. Because the structure of the nanopositioning stage is symmetric, the frequency response of the system is also symmetric as described in Fig. 4. It can be seen the cross coupling in non-diagonal plots are achieved from −65 dB to −20 dB at low frequency (from 1 Hz to 70 Hz). However, the magnitude tends to be positive with the increase of scan speed, which results in strong cross coupling effect on tracking, especially at the resonant frequency of 123 Hz. This limits the positioning accuracy of the stage. The normalized transfer function of the MIMO system from the identification process is displayed in Eq. (23). When implementation in simulation, the normalized model and controllers were discretized by Tustin method with sampling interval of 0.0004 s.

$$\begin{cases} G_{xx} = \frac{146.6s^5 + 7.9\times10^5 s^4 + 9.8\times10^8 s^3 + 2.1\times10^{12} s^2 + 7.3\times10^{14} s + 9.4\times10^{17}}{s^6 + 1009s^5 + 3.8\times10^6 s^4 + 1.8\times10^9 s^3 + 3.5\times10^{12} s^2 + 7.1\times10^{14} s + 9.4\times10^{17}} \\ G_{xy} = \frac{104.1s^5 - 3.6\times10^4 s^4 + 8.9\times10^7 s^3 - 1.7\times10^{11} s^2 + 8.2\times10^{13} s - 1.6\times10^4}{s^6 + 1009s^5 + 3.8\times10^6 s^4 + 1.8\times10^9 s^3 + 3.5\times10^{12} s^2 + 7.1\times10^{14} s + 9.4\times10^{17}} \\ G_{yx} = \frac{104.1s^5 - 3.6\times10^4 s^4 + 8.9\times10^7 s^3 - 1.7\times10^{11} s^2 + 8.2\times10^{13} s - 1.6\times10^4}{s^6 + 1009s^5 + 3.8\times10^6 s^4 + 1.8\times10^9 s^3 + 3.5\times10^{12} s^2 + 7.1\times10^{14} s + 9.4\times10^{17}} \\ G_{yy} = \frac{146.6s^5 + 7.9\times10^5 s^4 + 9.8\times10^8 s^3 + 2.1\times10^{12} s^2 + 7.3\times10^{14} s + 9.4\times10^{17}}{s^6 + 1009s^5 + 3.8\times10^6 s^4 + 1.8\times10^9 s^3 + 3.5\times10^{12} s^2 + 7.1\times10^{14} s + 9.4\times10^{17}} \end{cases} \quad (23)$$

4.2 Suppression of Cross-Coupling Effect

To evaluate the effect of DDFDF for eliminating cross-coupling errors, triangle signals with difference frequencies are input into x axis and the output data from y axis were measured to obtain cross-coupling errors. Figure 5 shows the cross-coupling errors with the 10 Hz, 20 Hz, 50 Hz and 80 Hz triangle input for y axis with the peak-to-peak amplitude of 2 μm. It can be observed that the cross-coupling errors increase with the input frequencies increasing. At low frequency of 10 Hz, the RMS error is below 13 nm and the MAX error is below 35 nm. However, the errors with FB & DDFDF are 7 nm for RMS and 16 nm for MAX from 10 Hz to 50 Hz which verifies the effect of MFDF to suppress cross-coupling errors. The RMS errors and MAX errors for y axis were recorded in Table 1. We should note that at 40 Hz, the cross-coupling errors of open-loop and FB are larger than 50 Hz because the resonant frequency of non-diagonal term is 123 Hz, which is about twofold of fundamental frequency for the

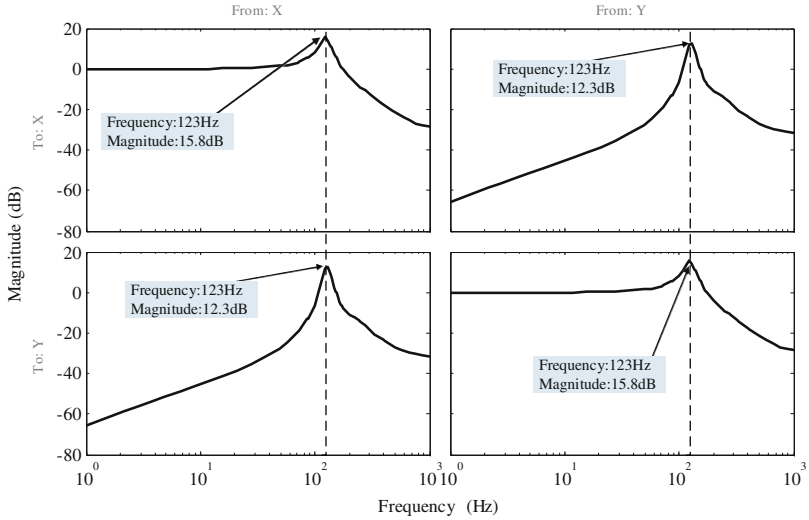

Fig. 4. Frequency responses of the stage. The resonant peak is 15.8 dB at 123 Hz for diagonal frequency responses and 12.3 dB at 123 Hz for non-diagonal frequency responses.

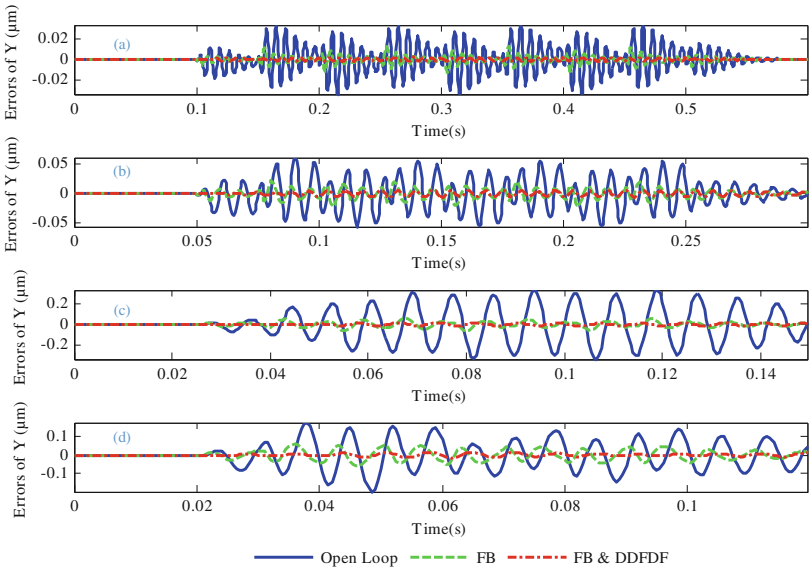

Fig. 5. Cross-coupling errors of *y* axis. (a) 10 Hz triangle. (b) 20 Hz triangle. (c) 40 Hz triangle. (d) 50 Hz triangle.

40 Hz input. At higher frequency of 50 Hz, the proposed control strategy reduces the RMS errors by 92.09 % (from 76.32 nm to 6.04 nm) and 76.74 % (from 25.97 nm to 6.04 nm) with respect to open-loop and FB, respectively.

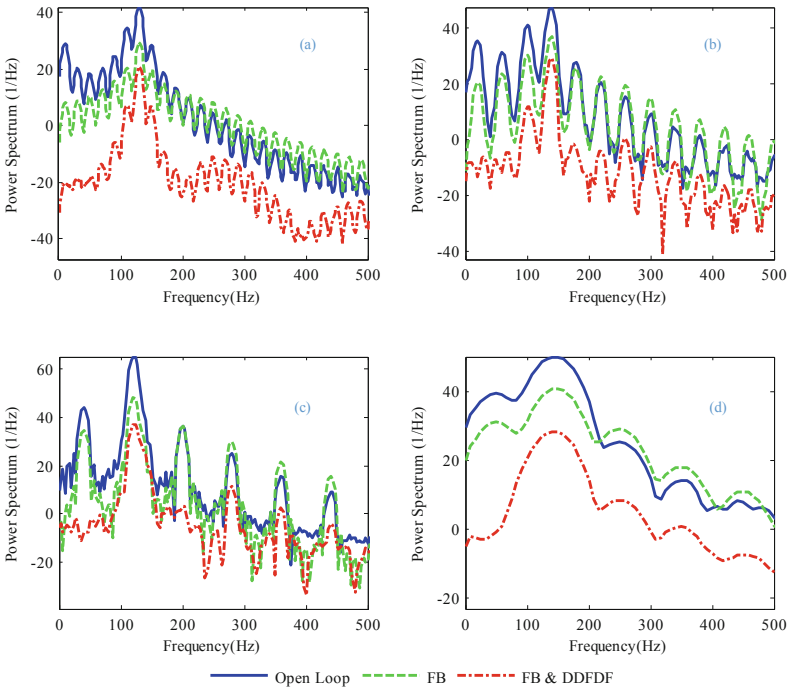

Fig. 6. Power spectrum of errors. (a) 10 Hz triangle. (b) 20 Hz triangle. (c) 40 Hz triangle. (d) 50 Hz triangle

The power spectrums of errors are presented in Fig. 6. It can be seen that the power with proposed controller are the lowest than others, although near the first resonant frequency, which verifies the ability to suppress the cross-coupling effect.

Table 1. Cross-coupling errors of *y* axis

Controller	Statistical errors(nm)	Triangle wave			
		10 Hz	20 Hz	40 Hz	50 Hz
Open Loop	RMS	12.85	25.19	167.00	76.32
	MAX	34.80	62.59	338.31	197.84
FB	RMS	3.13	7.56	23.14	25.97
	MAX	12.60	22.21	62.47	57.30
FB&DDFDF	RMS	1.01	2.95	5.92	6.04
	MAX	2.27	6.37	15.53	15.41

5 Conclusions

In this paper, the data-driven feedforward decoupling filter was introduced to compensate errors resulting from cross-coupling effects for coupled parallel piezo nanopositioning stages. The coefficients of DDFDF were obtained by Gauss-Newton gradient-based

algorithm with the superiority of no need for accurate identified model and model structure. The simulations based on a parallel piezo nanopositioning stage show that cross-coupling errors were suppressed significantly especially at high frequencies by implementing DDFDF when input signals of one axis were triangle wave with different frequencies.

Acknowledgments. This research was sponsored by National Natural Science Foundation of China (NSFC, Grant No.51375349).

References

1. Devasia, S., Eleftheriou, E., Moheimani, S.O.R.: A survey of control issues in nanopositioning. IEEE Trans. Control Syst. Technol. **15**(5), 802–823 (2007)
2. Salapaka, S.M., Salapaka, M.V.: Scanning probe microscopy. IEEE Control Syst. **28**(2), 65–83 (2008)
3. Binnig, G., Quate, C.F., Gerber, C.: Atomic force microscope. Phys. Rev. Lett. **56**(9), 930 (1986)
4. Rakotondrabe, M., Haddab, Y., Lutz, P.: Development, modeling, and control of a micro-/nanopositioning 2-DOF stick–slip device. IEEE/ASME Trans. Mechatron. **14**(6), 733–745 (2009)
5. Yong, Y.K., Moheimani, S.O.R., Kenton, B.J., et al.: Invited review article: High-speed flexure-guided nanopositioning: Mechanical design and control issues. Rev. Sci. Instrum. **83**(12), 121101 (2012)
6. Kenton, B.J., Leang, K.K.: Design and control of a three-axis serial-kinematic high-bandwidth nanopositioner. IEEE/ASME Trans. Mechatron. **17**(2), 356–369 (2012)
7. Bhikkaji, B., Ratnam, M., Moheimani, S.O.R.: PVPF control of piezoelectric tube scanners. Sens. Actuators A **135**(2), 700–712 (2007)
8. Li, Y., Xu, Q.: Development and assessment of a novel decoupled XY parallel micropositioning platform. IEEE/ASME Trans. Mechatron. **15**(1), 125–135 (2010)
9. Yao, Q., Dong, J., Ferreira, P.M.: Design, analysis, fabrication and testing of a parallel-kinematic micropositioning XY stage. Int. J. Mach. Tools Manuf. **47**(6), 946–961 (2007)
10. Das, S.K., Pota, H.R., Petersen, I.R.: Multivariable negative-imaginary controller design for damping and cross coupling reduction of nanopositioners: a reference model matching approach. IEEE/ASME Trans. Mechatron. **20**(6), 3123–3134 (2015)
11. Das, S.K., Pota, H.R., Petersen, I.R.: A MIMO double resonant controller design for nanopositioners. IEEE Trans. Nanotechnol. **14**(2), 224–237 (2015)
12. Das, S.K., Pota, H.R., Petersen, I.R.: Resonant controller design for a piezoelectric tube scanner: a mixed negative-imaginary and small-gain approach. IEEE Trans. Control Syst. Technol. **22**(5), 1899–1906 (2014)
13. Yong, Y.K., Liu, K., Moheimani, S.O.R.: Reducing cross-coupling in a compliant XY nanopositioner for fast and accurate raster scanning. IEEE Trans. Control Syst. Technol. **18**(5), 1172–1179 (2010)
14. Hjalmarsson, H., Gevers, M., Gunnarsson, S., et al.: Iterative feedback tuning: theory and applications. IEEE Control Syst. **18**(4), 26–41 (1998)
15. Hjalmarsson, H.: Efficient tuning of linear multivariable controllers using iterative feedback tuning. Int. J. Adapt. Control Signal Process. **13**(7), 553–572 (1999)

16. Campi, M.C., Lecchini, A., Savaresi, S.M.: Virtual reference feedback tuning: a direct method for the design of feedback controllers. Automatica **38**(8), 1337–1346 (2002)
17. Campi, M.C., Lecchini, A., Savaresi, S.M.: An application of the virtual reference feedback tuning method to a benchmark problem. Eur. J. Control **9**(1), 66–76 (2003)
18. Zheng, J., Guo, G., Wang, Y.: Feedforward decoupling control design for dual-actuator system in hard disk drives. IEEE Trans. Magn. **40**(4), 2080–2082 (2004)
19. Boyd, S., Vandenberghe, L.: Convex Optimization. Cambridge University Press, Cambridge (2004)
20. Teo, Y.R., Eielsen, A.A., Gravdahl, J.T., et al.: Discrete-time repetitive control with model-less FIR filter inversion for high performance nanopositioning. In: IEEE/ASME International Conference on Advanced Intelligent Mechatronics (AIM), pp. 1664–1669 (2014)
21. Hu, C., Yao, B., Wang, Q.: Coordinated adaptive robust contouring control of an industrial biaxial precision gantry with cogging force compensations. IEEE Trans. Industr. Electron. **57**(5), 1746–1754 (2010)
22. Chen, C.S., Chen, L.Y.: Robust cross-coupling synchronous control by shaping position commands in multiaxes system. IEEE Trans. Industr. Electron. **59**(12), 4761–4773 (2012)
23. Skogestad, S., Postlethwaite, I.: Multivariable Feedback Control: Analysis and Design. Wiley, New York (2007)
24. Huusom, J.K., Poulsen, N.K., Jørgensen, S.B.: Improving convergence of iterative feedback tuning. J. Process Control **19**(4), 570–578 (2009)